

## Electron-diffraction and photoelectron-spectroscopy studies of fullerene and alkali-metal fulleride films

P. J. Benning, F. Stepniak, and J. H. Weaver

*Department of Materials Science and Chemical Engineering, University of Minnesota, Minneapolis, Minnesota 55455*

(Received 17 May 1993)

Photoelectron spectroscopy and low-energy electron diffraction (LEED) have been used to examine the electronic structure and crystallinity of thin films of  $A_xC_{60}$  where  $A = \text{Na, K, Rb, and Cs}$  and  $0 \leq x \leq 6$ . For undoped  $C_{60}$  films, temperature-dependent LEED studies show changes that correspond to the lattice transformation from the simple-cubic to the face-centered-cubic structure. For doped  $C_{60}$  films, the LEED results show a decrease in the quality of the LEED pattern upon the nucleation of the body-centered  $A-C_{60}$  phases. Spectroscopic studies of these fullerides indicate that the effects of electron correlation are always important. In particular, the  $A_1C_{60}$  phases of Rb and Cs are characterized by an occupied-valence-band feature  $\sim 0.5$  eV wide centered  $\sim 0.25$  eV below  $E_F$  that is derived from the lowest unoccupied molecular orbitals (LUMO) of  $C_{60}$ . The much greater width relative to band calculations is attributed to electron correlation. For these phases, there is also emission at the Fermi level, despite the fact that transport studies indicate insulating character. This implies that the electronic states at  $E_F$  are localized. The  $A_3C_{60}$  phase of K and Rb exhibit a metallic Fermi-level cutoff. Spectroscopic features 0.3 and 0.7 eV below  $E_F$  are also observed that are not reproduced in one-electron band-structure calculations. The  $A_4C_{60}$  phases of K, Rb, and Cs all exhibit insulating character with a split LUMO band. All of the  $A_6C_{60}$  phases are insulators with a filled LUMO band. For Na- $C_{60}$ , the valence-band spectra show no emission at  $E_F$  for any Na concentration. Finally, photoemission results showed partial occupation of the (LUMO+1)-derived levels, corresponding to  $C_{60}^{8-}$  for isolated  $C_{60}$  molecules deposited onto multilayers of Na, K, and Rb at 40 K.

### I. INTRODUCTION

Studies of the alkali-metal fullerides have revealed a rich array of ordering transitions<sup>1-8</sup> and electronic<sup>9-11</sup> and transport properties.<sup>12,13</sup> In particular, it has been shown that incorporation of alkali-metal atoms into the interstitial sites of the fullerene lattice results in distinct fulleride phases, some based on the face-centered-cubic fullerene lattice and others based on the body-centered fullerene lattices.<sup>3-8</sup> Photoemission investigations have shown that each fulleride phase has distinct electronic characteristics but the details of the electronic structure near the Fermi level ( $E_F$ ) in the different phases remain controversial.<sup>10</sup>

In this paper, we present high-resolution valence-band photoemission results for highly ordered  $C_{60}$  and  $A_xC_{60}$  films ( $A = \text{Na, K, Rb, Cs}$ ) that reveal the spectroscopic signatures of the different fulleride phases. These results show the occupation of a feature derived from the lowest unoccupied molecular orbital (LUMO) for each alkali metal but also differences that reflect the specifics of the phase diagrams for these systems. Photoemission spectra for nonmetallic  $Rb_xC_{60}$  and  $Cs_xC_{60}$  films with  $x \sim 1$  show a nearly Gaussian-shaped LUMO-derived feature  $\sim 0.5$  eV wide that is centered  $\sim 0.25$  eV below  $E_F$ . The band is much wider than predicted by one-electron band-structure calculations, and this broadening is attributed to electron correlation. The electronic states at  $E_F$  are localized. This may reflect merohedral rearrangement of the  $C_{60}$  molecules in the  $A_1C_{60}$  films.<sup>1,4</sup> In addition,

there may be contributions due to disorder in the octahedral site occupancy. From spectroscopic investigations,<sup>4</sup> it is known that Rb and Cs ions occupy only octahedral sites for  $x \leq 1$  but the concentration of octahedral vacancies for  $0 \leq x \leq 1$  is not known. For the metallic  $K_3C_{60}$  and  $Rb_3C_{60}$  phases, there is a well-defined Fermi-level cutoff but the LUMO-derived features are again much broader than predicted by one-electron band calculations. For the  $x = 4$  phases of K, Rb, and Cs, there are no states near  $E_F$ , and the electronic properties resemble those of a Mott insulator. For Na- $C_{60}$ , the photoemission results show no emission at  $E_F$  for any stoichiometry and the results for  $x = 6$  are equivalent to those for the bcc-based  $A_6C_{60}$  fullerides.

Low-energy electron-diffraction studies of  $C_{60}$  films at 40 K reveal a hexagonal pattern consistent with a simple-cubic crystal structure that has a basis of four molecules, as observed in x-ray-diffraction studies.<sup>3</sup> Temperature-dependent studies reveal a structural transition for the surface mesh at  $230 \pm 20$  K that corresponds to the lattice transformation from simple cubic to the fcc phase for the surface mesh that occurs at  $230 \pm 20$  K. LEED studies for the doped fullerides show a hexagonal pattern corresponding to the (111) surface of the fcc-based fullerides. They also indicate structural transitions for K- $C_{60}$  and Rb- $C_{60}$  for  $x$  near 3 and for Cs- $C_{60}$  for  $x$  near 1 as the body-centered-tetragonal  $A_4C_{60}$  structures form. No changes from the fcc structure were observed for Na- $C_{60}$  at any stoichiometry. Finally, to investigate the possibility that the fullerenes could accept more than

six electrons, we deposited submonolayer amounts of  $C_{60}$  onto Na, K, and Rb multilayer films at 40 K. Photoemission results showed complete occupation of the LUMO levels (six electrons) and the partial occupation of the LUMO+1 levels (two electrons), indicating  $C_{60}^{8-}$  charge states.

## II. EXPERIMENT

Fullerene films were grown with  $C_{60}$  sublimed from Ta boats in ultrahigh vacuum. The films were formed on cleaved GaAs(110) surfaces held at 180°C. Attempts to grow films on substrates heated an additional 20°C were unsuccessful because the sticking coefficient was less than 0.01. At 180°C, the sticking coefficient was  $\sim 0.2$ , as determined by comparing the measured rate of attenuation of the GaAs substrate core-level emission with the film thicknesses determined using a quartz-crystal thickness monitor. In general, the films studied were  $\sim 200$  Å. The temperatures during growth and annealing were measured with a chromel-alumel thermocouple attached to the base of the GaAs posts. Although the estimated uncertainty in absolute temperature is  $\pm 20$ °C, the relative uncertainty between two measurements is much smaller, approximately  $\pm 5$ °C. Scanning-tunneling-microscopy (STM) studies of films grown under the same conditions showed grain dimensions that were greater than  $\sim 3500$  Å with the quality of the  $C_{60}$  films determined by the perfection of the cleaved GaAs surface. Previous spectroscopic studies of GaAs(110) surfaces produced in this way have shown a flatband condition with the Fermi-level position near the band edge. Additional studies have examined  $C_{60}$  growth on GaAs(110) surfaces that contained a high step density in the  $[\bar{1}12]$  direction. In this case, there were different constraints on  $C_{60}$  film orientation, because the steps acted as nucleation centers.

The fulleride films were formed by exposing ordered  $C_{60}$  films to alkali-metal atoms from carefully degassed SAES getter sources. During doping, the  $C_{60}$  films were held at 180°C and the pressures were below  $2 \times 10^{-10}$  Torr. The alkali-metal concentrations were determined from core-level and LUMO emission intensities, assuming that the final or saturated composition was  $A_6C_{60}$  for each fulleride. This assumption was based on the observation that the LUMO level was fully occupied at saturation, accounting for the transfer of six electrons to each fullerene. Such analysis gives  $x$  with an estimated uncertainty of  $\pm 0.2$ .

The x-ray photoemission spectroscopy (XPS,  $h\nu = 1486.6$  eV), He I ultraviolet photoemission spectroscopy (UPS,  $h\nu = 21.2$  eV), and LEED measurements were conducted in an ultrahigh vacuum system with a base pressure of  $7 \times 10^{-11}$  Torr. The total-energy resolution, defined as the energy interval over which the emission intensity at  $E_F$  drops from 90% to 10% of the maximum intensity, is 100 meV for the UPS spectra presented here. For the XPS measurements, the full width at half maximum of the C 1s main line was 1.25 eV. A closed-cycle helium refrigerator was attached to the sample holder via a copper braid to cool below room temperature. The lowest temperature was  $\sim 40$  K. LEED studies were con-

ducted using a 4-grid Varian system with a phosphor screen detector. Heating was done with a tungsten filament heater.

## III. RESULTS AND DISCUSSION

### A. $A-C_{60}$ and $C_{60}$ structure

It is now generally accepted that the fullerides exhibit distinct phases,  $A_nC_{60}$ , where  $n$  is 1, 2, 3, 4, or 6, depending on the alkali-metal species.<sup>10,11</sup> For stoichiometries between these values, the films will be mixed phase in character as required by the Gibbs phase rule with the amounts of the appropriate line phases dictated by the lever rule. It has been shown, however, that kinetic constraints limit the approach to thermodynamic equilibrium for fulleride growth by pulse deposition in ultrahigh vacuum.<sup>14</sup> For example, studies of  $K_xC_{60}$  have shown that  $K_3C_{60}$  and  $K_4C_{60}$  phases coexist before the global stoichiometry reaches  $x = 3$ , despite thermodynamic arguments to the contrary.

To assess the quality of our films, to insure their crystallinity, and to study structural changes associated with alkali-metal incorporation, we undertook temperature-dependent LEED measurements. Previous STM and LEED studies in a separate system have provided additional confidence in our characterization of film quality. In general, we have observed LEED patterns of fulleride films for electron energies from 25 to above 200 eV. The spacings of the GaAs(110) spots determined prior to  $C_{60}$  film growth were used to determine the size of the  $C_{60}$  surface cell. For pure  $C_{60}$ , it was necessary to use relatively low electron energies, 25 eV, to obtain patterns near 300 K because of the intrinsic orientational disorder of the fullerenes, as discussed below.

Figure 1(a) shows a LEED pattern from a 200-Å film of  $K_{0.1}C_{60}$  at 40 K. The GaAs(110) substrate  $[1\bar{1}0]$  and  $[001]$  directions are defined at the bottom. The electron energy was 60 eV, giving a wave number of  $3.7 \text{ \AA}^{-1}$ , and the electron spot size was  $\sim 1 \text{ mm}^2$ . The (00) spot is seen to the left of the LEED gun as a result of off-normal incidence of the LEED electrons. The doping level of  $x = 0.1$  is slightly above the solid solubility of K in  $C_{60}$  so that small amounts of  $K_3C_{60}$  have started to form but the film is still overwhelmingly  $\alpha-C_{60}(K)$ . The LEED pattern for this solid solution phase is indistinguishable from that of pure  $C_{60}$ . In particular, the hexagonal pattern and spot separation indicate a surface net with  $20 \pm 1$  Å spacings, consistent with a simple-cubic structure having a basis of four molecules with lattice points separated by 20.08 Å, as has been demonstrated by  $C_{60}$  below 249 K.<sup>1</sup>

The orientation of the  $C_{60}$  LEED pattern in relation to the GaAs(110) substrate pattern indicates that the  $C_{60}$  grains grow with an  $\sim 3.5^\circ$  misorientation between  $C_{60}[1\bar{1}0]$  and GaAs $[1\bar{1}1]$ , producing a structure that is incommensurate with the substrate. This rotation is consistent with STM results that showed that (strained) commensurate  $C_{60}$  films would grow in patches for submonolayer coverages.<sup>15</sup> A  $C_{60}$  lattice rotation of  $\pm 3.5^\circ$  will produce a more nearly perfect unstrained close-packed film that is incommensurate with GaAs(110). Domains

of each orientation will be produced by nucleation on the GaAs surface and these domains will coalesce to produce slightly misoriented domains, as shown by STM images.<sup>16</sup> This two-domain character is evident by the doubling of the LEED spots. For comparison, the schematic in Fig. 1(b) represents two hexagonal patterns with  $\pm 3.5^\circ$  rotations. A moiré pattern created by the overlap of the two simple-cubic patterns with a relative rotation of  $7^\circ$  produces the bright and dim patches separated by  $60^\circ$  near the periphery of the LEED screen of Fig. 1(a), as demonstrated in Fig. 1(b).

Figure 1(c) shows the LEED pattern at 40 K for  $K_xC_{60}$  where  $x = 2.2$ . At this stage of doping, the sample should show a mixture of grains of  $\alpha\text{-}C_{60}(K)$  and  $K_3C_{60}$ . Inspection shows that the smaller hexagons, defined by the half-order spots, are no longer visible. These half-order spots are characteristic of the simple-cubic structure with its larger lattice constant. Their disappearance is expected because the  $K_3C_{60}$  grains dominate at this stoichiometry. The larger hexagons indicate a  $10 \pm 1 \text{ \AA}$

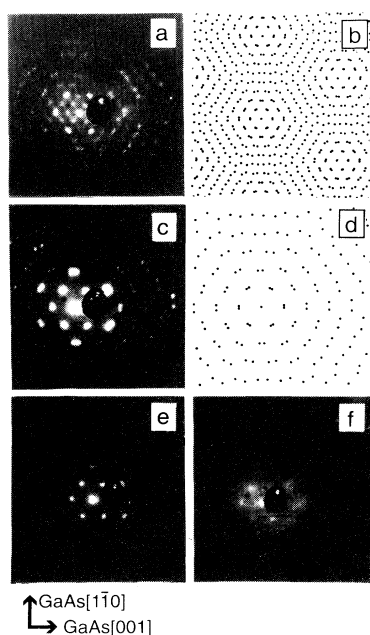


FIG. 1. LEED results at 40 K from a highly ordered  $K\text{-}C_{60}$  film grown on GaAs(110) (electron energy 60 eV, film thickness 200 Å). (a) The hexagonal LEED pattern of  $K_{0.1}C_{60}$  is indicative of the simple-cubic lattice of  $C_{60}$  at 40 K. A moiré pattern is produced for growth on step-free surfaces because domains of  $C_{60}(111)$  can optimize substrate registry with  $[1\bar{1}0]$  oriented at  $\pm 3.5^\circ$  relative to GaAs $[1\bar{1}1]$ . This moiré pattern produces the dim and bright areas in (a) and the effect is modeled schematically in (b) where two simple-cubic arrays are rotated  $7^\circ$  relative to one another. (c) The LEED pattern for  $x = 2.2$  shows that the simple-cubic pattern is lost as the fcc  $K_3C_{60}$  pattern, characterized by the larger hexagons, increases. Again, the patterns from domains rotated  $\pm 3.5^\circ$  are clearly evident in (c). They are represented schematically in (d) where there are two spots for each hexagonal net position. The LEED pattern deteriorates as K concentration is increased to 2.8 and 3.7 and the  $K_3C_{60}$  grains are converted to body-centered  $K_4C_{60}$  grains.

lattice spacing that is consistent with the fcc  $K_3C_{60}(111)$  structure. Figure 1(d) shows a schematic of two hexagonal patterns rotated by  $7^\circ$ , corresponding to the fcc LEED pattern of Fig. 1(c). No moiré pattern is produced on the screen for the larger hexagons but the double spots are clearly evident.

Variations in the intensities of the LEED spots relative to the background provide a measure of the surface structural disorder and the mixture of the two (or more) phases present.<sup>17</sup> Continued deposition of K beyond that represented by Fig. 1(c) reduces the quality of the LEED pattern. This reflects the growth of  $K_4C_{60}$  grains on extended terraces of  $K_3C_{60}(111)$ . As discussed elsewhere based on photoemission results,<sup>12,14</sup> the formation of  $K_4C_{60}$  at the surface occurs for global stoichiometries below  $x = 3$  because true thermodynamic equilibrium cannot be achieved by vapor phase growth *in vacuo*.

Figures 1(e) and 1(f) show the effects of doping to  $x = 2.8$  and 3.7, respectively, where the growth of the  $K_4C_{60}$  phase markedly reduces the quality of the LEED pattern. The lack of a discernible LEED pattern in these studies for stoichiometries above  $x = 4$  can be explained in terms of surface disorder introduced by the lattice expansion associated with the fcc to bct phase transition. The surface disorder introduces random-phase shifts in the diffracted electron wave functions, reducing the spot intensities.<sup>17</sup>

LEED studies were also carried out on Na, Rb, and Cs fulleride films grown under conditions identical to those of  $K\text{-}C_{60}$ . These studies demonstrated that highly ordered films could be produced, with differences that reflect the phase diagrams of the respective alkali-metal fullerenes. For Rb- $C_{60}$ , the LEED results were similar to those of  $K\text{-}C_{60}$ , showing the highest-quality fcc pattern for  $x$  near 2, a reduction in quality for  $x$  approaching 4, and then the loss of a discernible pattern. In studies conducted at 40 K, the simple-cubic pattern was greatly reduced at  $x = 0.4$ , consistent with the formation of a fcc  $Rb_1C_{60}$  phase. For Cs- $C_{60}$ , the LEED results showed that the low-temperature simple-cubic pattern disappeared as the fcc  $A_1C_{60}$  phase grew, but the fcc pattern faded quickly after  $x = 1$ . The disappearance of the  $A_1C_{60}$  fcc pattern in  $Cs_xC_{60}$  for lower  $x$  than in  $Rb_xC_{60}$  and  $K_xC_{60}$  reflects the fact that doping beyond  $x = 1$  results in the nucleation of a body-centered phase (a  $Cs_3C_{60}$  phase does not exist<sup>5</sup>). Finally, the Na- $C_{60}$  results were unique in that the fcc pattern persisted until  $x = 6$ . This is in good agreement with studies of the bulk structure<sup>18</sup> where the fcc structure is maintained for all alkali-metal concentrations. For Na- $C_{60}$ , there is multiple occupancy of the octahedral site for  $x > 3$  so that the transformation to a body-centered phase does not occur.

## B. Temperature-dependent LEED of $C_{60}$

Early structural studies of pure  $C_{60}$  showed an ordering transition at 249 K that involved a fcc to simple-cubic transformation.<sup>2</sup> The structural transition is associated with a change in the basis from one molecule to four. Above 249 K, the molecules are orientationally disordered, with rotational diffusion between symmetry-

inequivalent positions. The orientational ordering has been shown to be dynamic in bulk studies<sup>2</sup> with the molecules ratcheting between symmetry-equivalent positions below 249 K.

Figure 2 shows LEED patterns obtained for a 100-Å-thick  $C_{60}$  film using 25-eV electrons ( $k=2.56 \text{ \AA}^{-1}$ ). The (00) spot is now seen directly above the electron gun. The pattern of Fig. 2(a) differs from that of Fig. 1 because it shows a single hexagonal pattern with  $C_{60}[\bar{1}10]$  aligned with  $\text{GaAs}[\bar{1}12]$  rather than two hexagonal patterns with a  $7^\circ$  rotation between them. The single orientation is obtained by growing the film on a heavily stepped  $\text{GaAs}(110)$  surface. Evidence of a stepped surface was seen in the LEED spots of the  $\text{GaAs}$  surface. The spots were elongated in the  $\text{GaAs}[\bar{1}12]$  direction, indicating steps in this direction with terrace widths less than the  $\sim 100\text{-\AA}$  coherence length of our LEED system.<sup>17</sup> Scanning-tunneling-microscopy studies have shown<sup>15</sup> that close-packed  $\langle 110 \rangle$  directions of  $C_{60}$  overlayers form along  $\text{GaAs}$  steps and the layers grow outward from the step-by-step flow. A high density of  $\text{GaAs}[\bar{1}12]$  steps will force an alignment of  $\text{GaAs}[\bar{1}12]$  and  $C_{60}[\bar{1}10]$ , giving the orientation observed in Fig. 2.  $C_{60}$  alignment with the step edges avoids the  $\pm 3.5^\circ$  rotation that dominates when the step separation is large and nucleation occurs on the terraces. Even so, we do see a slight rotational misalignment between grains, giving rise to the elongated spots near the edges of the screen in Figs. 2(a)–2(d). The  $C_{60}$  LEED pattern does not vary across the  $4 \times 4 \text{ mm}^2$  surface, indicating aligned grains and a well-ordered surface.

The images of Figs. 2(a)–2(d) show the  $C_{60}$  LEED pattern obtained at 40, 110, 200, and 230 K (electron energy 25 eV). The separation of the spots at low temperature indicates a surface cell with a lattice constant of  $20 \pm 1 \text{ \AA}$

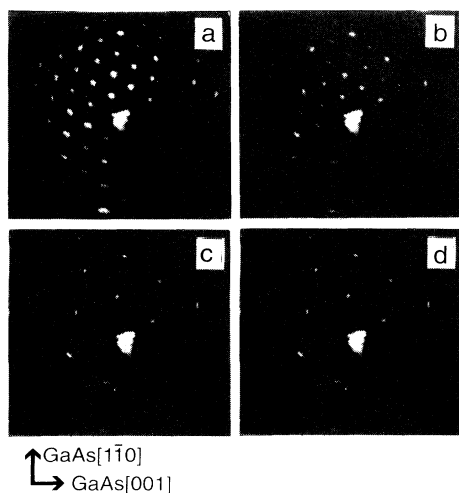


FIG. 2. (a)–(d) LEED results for undoped  $C_{60}$  at 40, 110, 200, and 230 K showing the washing out of the half-order spots with increasing temperature (electron energy 25 eV, film thickness 100 Å). The reduction is a consequence of increased librational motion above  $\sim 90 \text{ K}$  and the reduction in the simple-cubic order parameter.

in the close-packed  $\langle 110 \rangle$  directions, as expected for simple cubic  $C_{60}(111)$ . As the temperature is raised from 40 K, the intensities of the spots diminish. The intensity changes are a result of enhanced incoherent scattering as the librational amplitude grows. This can be understood in terms of a rotational Debye-Waller factor  $\exp[-(\mathbf{u} \cdot \Delta \mathbf{k})^2]$ , where  $\mathbf{u}$  is the displacement from equilibrium of a carbon atom scattering site due to librational motion.<sup>19</sup>

Comparison of Figs. 2(a) and 2(d) shows that the smaller hexagons characteristic of the low-temperature  $C_{60}$  phase are not visible near 230 K and the pattern of larger hexagons persists to 300 K. The loss of the half-order spot intensity reflects the reduction in the simple-cubic order parameter, as expected given the bulk phase transformation of  $C_{60}$ .<sup>2</sup> The transition to the disordered phase that can be determined visually from the LEED pattern occurs at  $230 \pm 20 \text{ K}$ . Given the uncertainty in temperature, one should be cautious in concluding that the molecules become disordered at a temperature below the bulk transition of 249 K, although, in principle, a lower transition temperature would be possible because surface molecules have fewer neighbors to impede rotational diffusion.

Temperature-dependent LEED studies of undoped  $C_{60}(111)$  with 60-eV electrons showed the disappearance of all spots at  $\sim 230 \text{ K}$ . Equivalent studies of fcc  $\text{K}_3\text{C}_{60}(111)$  showed a clear pattern at 300 K. This indicates that the K ions impose an ordering of the surface molecules. For the undoped films, the loss of LEED intensity can be understood in terms of the reduction of coherence in the scattered waves because of phase differences introduced by atomic displacements from equilibrium. Inherent in the Debye-Waller effect is the fact that backscattered electrons with shorter wavelength (higher  $k$ ) experience larger phase shifts for the same average displacement,  $\langle u \rangle$ , and are more sensitive to the random orientation than forward-scattering probes such as x-ray diffraction, neutron diffraction, and transmission electron diffraction.<sup>19</sup> These three techniques, as well as LEED at 25 eV ( $k=2.56 \text{ \AA}^{-1}$ ), all have a smaller change in wave number upon diffraction than 60-eV electrons ( $k=3.70 \text{ \AA}^{-1}$ ). Thus, the fcc  $C_{60}(111)$  pattern is visible at 300 K only for low electron energies.

### C. $\text{K-C}_{60}$ spectroscopic results

Figure 3 shows valence-band spectra measured at 40 K from a highly ordered  $C_{60}$  film doped with K. The spectra, which are normalized to keep constant the height of the feature at  $\sim 4 \text{ eV}$ , are referenced to the grounded spectrometer Fermi level. Dilute doping induces an initial shift of the  $C_{60}$  features as  $E_F$  moves from a position 2.2 eV above the highest occupied molecular orbital (HOMO) center to a position near the conduction-band minimum, as for doping with any alkali metal.<sup>10,11</sup> Doping to  $x=0.1$  also produces a 1.5-eV-wide LUMO feature, a sharp cutoff at  $E_F$ , and a shoulder at  $\sim 1.6 \text{ eV}$ . The LUMO signatures are characteristic of  $\text{K}_3\text{C}_{60}$  (Ref. 9) and the shoulder corresponds to the leading portion of the HOMO for the  $\text{K}_3\text{C}_{60}$  phase. The appearance of emission from a  $\text{K}_3\text{C}_{60}$  minority phase suggests that the

solubility limit for the solid solution  $\alpha\text{-C}_{60}(\text{K})$  phase is below  $\text{K}_{0.1}\text{C}_{60}$ . The shape of the LUMO feature remains essentially unchanged for  $0.1 \leq x \leq 2.2$ , consistent with the existence of only the  $\alpha\text{-C}_{60}(\text{K})$  and  $\text{K}_3\text{C}_{60}$  phases below 425 K.<sup>4</sup> The HOMO- and (HOMO-1)-derived band of  $\text{K}_3\text{C}_{60}$  are shifted 0.6 eV relative to the corresponding levels of  $\alpha\text{-C}_{60}(\text{K})$  because  $E_F$  lies within the LUMO band. The superposition of emission from the two phases accounts for the broadening of the spectra. This broadening is particularly evident for  $\text{K}_{2.2}\text{C}_{60}$  where, from the lever rule, the sample should be  $\sim 70\%$   $\text{K}_3\text{C}_{60}$ . Since the spectra for  $0.1 \leq x \leq 2.2$  represent contributions from  $\alpha\text{-C}_{60}(\text{K})$  and  $\text{K}_3\text{C}_{60}$ , each with distinct line shapes and intensities determined from core-level analysis, it is possible to mathematically subtract the  $\alpha\text{-C}_{60}(\text{K})$  contribution, as discussed in Ref. 9 and shown in Fig. 4.

For  $x = 2.8$ , there is increased emission near  $\sim 0.5$  eV that signals the formation of the  $\text{K}_4\text{C}_{60}$  phase. This phase grows with K incorporation until there is no emission at  $E_F$  for  $x = 4.2$ . The  $x = 4.2$  spectrum provides the signature of the insulating  $\text{K}_4\text{C}_{60}$  phase.<sup>20</sup> LEED results

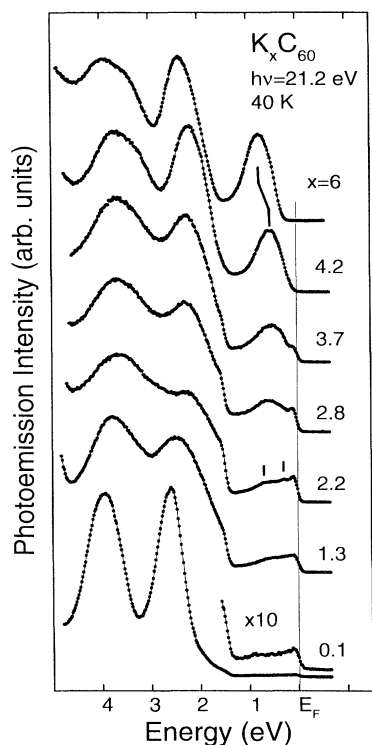


FIG. 3. Valence-band spectra of  $\text{K}_x\text{C}_{60}$  within 5 eV of  $E_F$  showing an increase in LUMO intensity with K concentration. The shape of the LUMO-derived band is largely unchanged for  $0.1 < x < 2.2$  because it originates from a single phase in this range of stoichiometries, as dictated by the K- $\text{C}_{60}$  phase diagram. The spectrum for  $x = 2.8$  shows enhanced emission at  $\sim 0.5$  eV as the insulating  $\text{K}_4\text{C}_{60}$  phase starts to form. The  $x = 4.2$  spectrum is derived almost entirely from  $\text{K}_4\text{C}_{60}$  and shows no emission at  $E_F$ . When the LUMO-derived band is completely filled, there is a shift of all features to higher binding energy.

confirm the disappearance of the fcc  $\text{K}_3\text{C}_{60}$  pattern at this concentration. Saturation doping to  $x = 6$  results in complete filling of the LUMO-derived band. When  $x$  reaches 6, the Fermi level is no longer pinned at the valence-band maximum by vacancy levels in the LUMO band. The resulting rigid shift in energy of all of the spectral features provides evidence of occupancy of the LUMO levels with few defects that would pin the Fermi level at the LUMO band edge.

Figure 4 compares the spectral signatures of  $\text{K}_3\text{C}_{60}$  and  $\text{K}_4\text{C}_{60}$  to calculations<sup>9</sup> of the density of states of these fullerenes. The  $\text{K}_3\text{C}_{60}$  curve was constructed by subtracting the  $\alpha\text{-C}_{60}(\text{K})$  HOMO and HOMO-1 features from the spectra for  $x = 2.2$  of Fig. 3. This  $\text{K}_3\text{C}_{60}$  curve (or the raw data, for that matter) shows a metallic cutoff at  $E_F$  but the LUMO feature is much broader than predicted by local-density-approximation (LDA) calculations (1.5 eV vs 0.3 eV).<sup>21,22</sup> The features at 0.3 and 0.7 eV cannot be related to band-structure effects. Instead, the 0.3-eV feature almost certainly reflects electronic coupling to vibronic modes of the fullerene, analogous to the Franck-Condon broadening observed for gas phase  $\text{C}_{60}$ .<sup>23</sup> The broad feature at 0.7 eV most likely reflects a transfer of spectral weight from the coherent part (at  $E_F$ ) to the

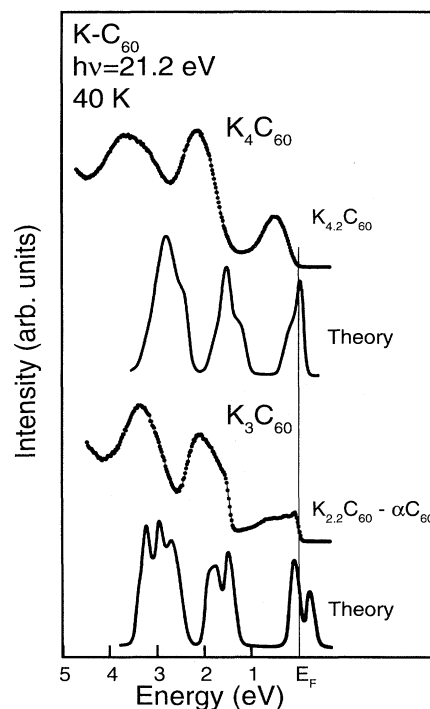


FIG. 4. Comparison of local-density calculations of the density of states of  $\text{K}_3\text{C}_{60}$  and  $\text{K}_4\text{C}_{60}$  with experiment showing good agreement for the HOMO-derived features but poor agreement for the band nearest  $E_F$ . The experimental  $\text{K}_3\text{C}_{60}$  curve was produced by subtracting the  $\alpha\text{-C}_{60}(\text{K})$  component from a  $\text{K}_{2.2}\text{C}_{60}$  spectrum where the amount subtracted was fixed by the  $x$  value. The discrepancies between theory and experiment reflect the importance of electron-electron correlation. For  $\text{K}_3\text{C}_{60}$ , there is a shift of spectral weight away from  $E_F$ . For  $\text{K}_4\text{C}_{60}$ , an insulating state is produced.

incoherent part of the spectral feature. This electron-correlation-induced broadening has also been observed in transition-metal oxides where the strength of the on-site Coulomb energy was related to the relative intensities of a narrow coherent feature at  $E_F$  and a broad incoherent feature below  $E_F$ .<sup>24,25</sup>

From Fig. 4 it is clear that the photoemission spectrum for  $K_4C_{60}$  is not at all what would be expected based on the independent-electron picture of filling of the three bands derived from the LUMO levels. In particular,  $K_4C_{60}$  seems to be an insulator, not a metal. The band splitting needed to produce an insulating state points to the importance of electron correlation in these narrow-band molecular solids. Transport measurements for high-quality K- $C_{60}$  films show that the resistivity is  $\sim 25$  m $\Omega$  cm for  $K_4C_{60}$ , about an order of magnitude higher than the typical limit for metals.<sup>26</sup> Likewise, temperature-dependent studies show the resistivity increases as temperature decreases (activated transport), indicating nonmetallic character.<sup>13</sup> The Mott-Hubbard splitting of the LUMO level then places  $K_4C_{60}$  on the insulating side of a metal-insulator transition. As will be shown below, electron-electron effects are also important in the  $A_1C_{60}$  phases when band broadening is again evident.

Knupfer *et al.*<sup>27</sup> have suggested that plasmon losses could account for the 0.7-eV feature of  $K_3C_{60}$ . They treated the many-body effects by considering coupling to an intrinsic charge-carrier plasmon rather than as a coherent and incoherent part of the spectral feature with weight distribution influenced by electron correlation. We suggest that models developed for metals or for insulators are close to their limits near the metal-insulator transition and neither may be strictly valid. Regardless of how the many-body effects are treated, however, it is clear that variations in stoichiometry place the  $A_3C_{60}$  structure on the metallic side of a metal-insulator transition and the other structures on the insulator side.

#### D. Rb- $C_{60}$ spectroscopic results

Figure 5 shows valence-band spectra for states within 5 eV of  $E_F$  for a highly ordered 200-Å film of  $Rb_xC_{60}$  for  $0.4 \leq x \leq 6$ . As for K- $C_{60}$ , the LUMO intensity evolves with alkali concentration until saturation at  $x=6$  when the valence-band features shift, as indicated, and  $E_F$  lies within the gap. There is an important difference compared to K- $C_{60}$ , however, because the  $Rb_1C_{60}$  phase is present even at low temperature.<sup>4</sup> ( $K_1C_{60}$  is formed only for  $T > 425$  K so that its signature is absent in the 40-K spectra.) The existence of a  $Rb_1C_{60}$  line phase requires that Rb incorporation beyond the solubility limit results in  $Rb_1C_{60}$  nucleation and two-phase coexistence, even for single-crystal starting materials. The presence of emission from the  $Rb_1C_{60}$  phase near  $E_F$  (discussed below) assures a different LUMO appearance from that seen for K- $C_{60}$  for low stoichiometries. Continued Rb incorporation produces metallic  $Rb_3C_{60}$  with a Fermi-level cutoff and features at 0.3 and 0.7 eV below  $E_F$ , as for  $K_3C_{60}$ . The  $Rb_4C_{60}$  phase nucleates before  $x=3$ , accounting for

the broad feature at  $\sim 0.5$  eV. The growth of the 0.5-eV feature and the changes in LUMO are clear in the spectrum for  $x=2.4$ . The spectrum for  $x=3.9$  corresponds to the highest stoichiometry with observable emission at  $E_F$ .<sup>20</sup> While it was relatively straightforward to decompose the spectral features for K- $C_{60}$  to obtain the signature of  $K_3C_{60}$ , it is more difficult (and not unique) for  $Rb_3C_{60}$  because the features of both  $Rb_1C_{60}$  and  $Rb_4C_{60}$  are present near  $x=3$ .

The nucleation of  $K_4C_{60}$  and  $Rb_4C_{60}$  occurs for global stoichiometries below  $x=3$  because of growth kinetics. While the Gibbs phase rule of equilibrium thermodynamics precludes three-phase coexistence, kinetic factors must be considered under vapor phase growth conditions at 180°C. The kinetics describe the diffusion of alkali-metal atoms on the surface or into the film and the different pathways that allow it to be incorporated into a fulleride phase. One pathway involves surface or bulk diffusion to edges of existing  $A_3C_{60}$  grains where incorporation would lead to grain growth and eventual conversion to a single crystal of  $A_3C_{60}$  (the equilibrium path-

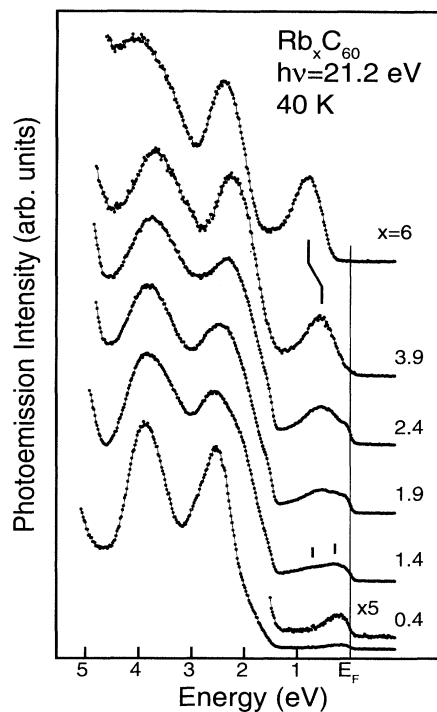


FIG. 5. Rb- $C_{60}$  valence-band features for a highly ordered film measured at 40 K (film thickness 200 Å). The  $x=0.4$  spectrum shows a LUMO feature indicative of a  $Rb_1C_{60}$  phase. The shoulder apparent at 1.9 eV in the  $x=0.4$  and 1.4 spectra corresponds to the  $Rb_1C_{60}$  HOMO emission. A new HOMO shoulder appears at 1.6 eV for  $x=1.9$ , indicative of the  $Rb_3C_{60}$  phase. The  $x=1.9$  spectrum also shows an increase in emission at 0.5 eV because of premature  $Rb_4C_{60}$  nucleation. Emission at  $E_F$  diminishes as the insulating  $Rb_4C_{60}$  grains grow until it is almost zero at  $x=3.9$ . Continued Rb incorporation produces the  $Rb_6C_{60}$  insulating state and results in a shift to higher binding energy of all the emission features.

way). The other describes the spontaneous formation of stable seeds of  $A_3C_{60}$  induced by alkali addition to  $A_3C_{60}$  surfaces. One should expect  $A_4C_{60}$  formation since the energy gain for alkali-metal incorporation is large ( $\sim 1.7$  eV/atom relative to the standard state<sup>9</sup>) and the surface will provide conditions that enhance  $A_4C_{60}$  transformation. Hence, kinetics would be important in dictating the microstructure and phase formation for the fullerides. The nucleation of  $A_4C_{60}$  at lower  $x$  for Rb than K (1.9 vs 2.5) is consistent with the larger size of Rb ions and the reduced bulk diffusivity of Rb through the fulleride film.

### E. Cs- $C_{60}$

Figure 6 shows the valence-band features for Cs- $C_{60}$ . Previous studies<sup>5</sup> have indicated that there is a stable  $Cs_1C_{60}$  phase at low temperature, that the  $Cs_3C_{60}$  phase is not formed, that the  $Cs_4C_{60}$  phase exhibits bct structure, and that saturation occurs at  $x=6$ . From Fig. 6, doping to  $Cs_{0.8}C_{60}$  reveals emission at  $E_F$  but the LUMO-derived emission is broader than predicted by one-electron band-structure calculations, though still narrow compared to the  $A_3C_{60}$  LUMO features of K- and Rb- $C_{60}$  (discussed below). In contrast to K- $C_{60}$  and Rb- $C_{60}$ , Cs incorporation after  $x \sim 1$  results in a *reduction* of emission at  $E_F$ , consistent with the absence of a metallic  $Cs_3C_{60}$  phase. Hence, incorporation past  $x=1$  produces a mixture of  $Cs_1C_{60}$  and insulating  $Cs_4C_{60}$ . The latter is typified by the

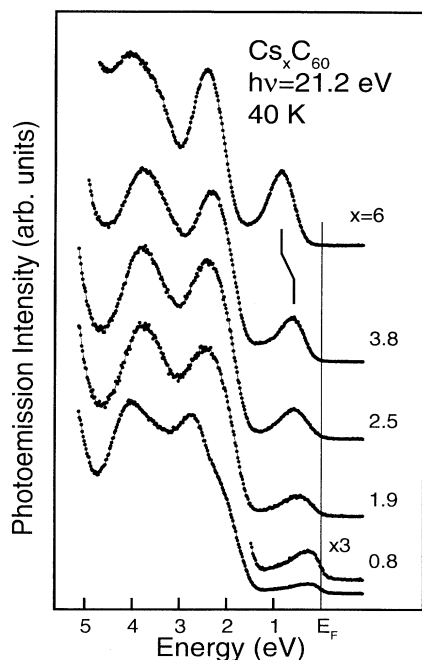


FIG. 6. Valence-band spectra for Cs- $C_{60}$  measured at 40 K. Doping to  $x=0.8$  produces a broad band at  $E_F$  and a shoulder near 1.9 eV. The shoulder is due to the HOMO band of the  $Cs_1C_{60}$  phase. The LUMO band broadening for  $x=1$  is related to electron correlation.  $Cs_1C_{60}$  is not metallic because the states at  $E_F$  are localized. Fermi-level emission is drastically reduced after  $x=1$  because no  $A_3C_{60}$  phase forms.

spectrum for  $x=3.8$ . LEED studies show that the fcc pattern fades quickly after  $x=1$ , as expected because the bct  $Cs_4C_{60}$  phase grows. The shoulder at  $\sim 2$  eV for  $x=0.8$  arises from the HOMO band of the  $Cs_1C_{60}$  phase, shifted 0.7 eV from the HOMO band of  $\alpha-C_{60}(Cs)$ . The  $Cs_6C_{60}$  spectrum at the top of Fig. 6 shows the customary shifting of fulleride valence-band features once the LUMO bands are filled and defect levels are eliminated. The fact that the  $A_4C_{60}$  phases of K, Rb, and Cs show no emission at  $E_F$  strongly suggests that the effects responsible for the insulating character are linked to the properties of the fullerenes and are relatively insensitive to the details of the extended lattice.

### F. Na- $C_{60}$

Figure 7 shows the valence-band emission within 5 eV of  $E_F$  for a 200-Å-thick  $Na_xC_{60}$  film for  $0.1 \leq x \leq 6$ . The spectra were acquired while the film was held at 450 K. The  $x=0.1$  spectrum shows a LUMO-derived feature that is nearly Gaussian in shape with a width of  $\sim 0.7$  eV centered at 0.6 eV. There is no emission at  $E_F$ . Continued Na incorporation produces an increase in LUMO emission at the same position and the growth of a corresponding HOMO feature at 2.2 eV. Saturation occurs at  $x=6$  with the familiar shift of all features to higher binding energy. Attempts to increase the Na content beyond  $x=6$  were unsuccessful under these growth conditions even though  $Na_{10}C_{60}$  samples have been produced under other conditions.<sup>28</sup> (LUMO+1 occupancy has been ob-

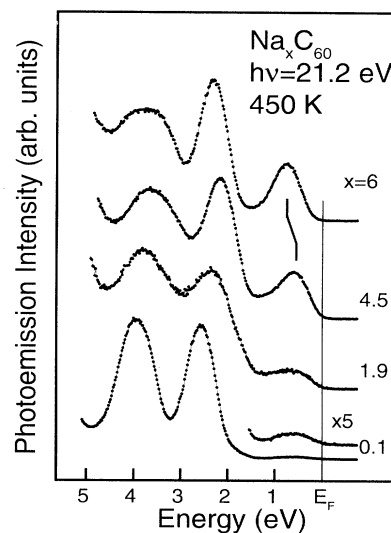


FIG. 7. Valence-band spectra for Na- $C_{60}$  measured at 450 K. In contrast to the other fullerides, doping with Na fails to produce a band with states at  $E_F$ . Instead, there is a band centered  $\sim 0.6$  eV below  $E_F$  that grows with  $x$ . Although  $Na_6C_{60}$  exhibits a fcc structure with multiple occupation of the octahedral hole, the valence-band spectrum of  $Na_6C_{60}$  is very similar to that for the saturated phases of the other fullerides. This emphasizes that it is the ionization state of  $C_{60}$  rather than the details of the arrangement of alkali-metal atoms that determines the electronic states of  $A_xC_{60}$  films.

served for  $C_{60}$  deposited on alkali-metal surfaces, as discussed in detail in Sec. III H.) LEED results indicate no change from the fcc host lattice for  $x > 4$ . This is consistent with previous structural studies<sup>18,28</sup> that report multiple occupancy of the octahedral site to obtain stoichiometries higher than  $Na_3C_{60}$ . Even with this unique structure, the valence-band spectra of  $Na_6C_{60}$  are very similar to those of the bcc  $A_6C_{60}$  components. The similarity for  $Na_6C_{60}$ ,  $Cs_6C_{60}$ ,  $Rb_6C_{60}$ , and  $K_6C_{60}$  again suggests the importance of the host molecular properties in determining the electronic characteristics of the fullerenes.

Emission at  $E_F$  was observed at low stoichiometries for K, Rb, and Cs fullerides, as discussed above, and its absence for Na- $C_{60}$  may be related to the unique structural properties of the Na- $C_{60}$  system. In particular, an  $A_2C_{60}$  phase with ions occupying the tetrahedral sites of the fcc host lattice has been reported only for Na- $C_{60}$ .<sup>18</sup> Hence, it is likely that the  $x = 0.1$  and 1.9 spectra of Fig. 7 represent emission from an insulating  $Na_2C_{60}$  phase. This suggests that correlation effects are more pronounced for the phases with an even number of electrons in the LUMO-derived bands (2 and 4) than the phases with odd  $x$  (1 and 3) where there is emission at  $E_F$ .

Valence-band spectra of several Na- $C_{60}$  films were also collected at 40 and 300 K but evidence of oxygen contamination was apparent at these temperatures.<sup>11</sup> In addition to O 1s emission we also observed a reduction in the LUMO feature at 0.6 eV and the growth of a new feature at 1.5 eV. We attribute the 1.5-eV feature to adsorbed NaO and/or NaOH on the fulleride surface. The 1.5-eV feature has been observed previously for other alkali-metal fulleride films but only after  $\sim 30$  h at 40 K. The differences suggest that the Na fulleride is less stable against oxides or hydrocarbon formation on the surface than the other alkali-metal fullerides.<sup>29</sup> No evidence of contamination was apparent at 450 K, indicating that the contaminants were volatile.

### G. $Rb_1C_{60}$ and $Cs_1C_{60}$

Figure 8 compares the LUMO-derived emission features at 40 K for  $K_{2.2}C_{60}$ ,  $Rb_{0.7}C_{60}$ , and  $Cs_{0.8}C_{60}$ , corresponding to stoichiometries at which the LUMO emission should be overwhelmingly  $K_3C_{60}$ ,  $Rb_1C_{60}$ , and  $Cs_1C_{60}$ , as labeled. The spectra are normalized to the maximum intensity of each curve to emphasize line-shape changes. For  $K_3C_{60}$  the integrated LUMO emission is  $\sim 3$  times that for  $Rb_1C_{60}$  and  $Cs_1C_{60}$ . The  $K_3C_{60}$  spectrum shows the broadening discussed above and features at 0.3 and 0.7 eV. The results for the  $A_1C_{60}$  phases show common features with a nearly Gaussian shaped peak  $\sim 0.5$  eV wide and an asymmetry to higher binding energy.

Comparison of the  $Rb_1C_{60}$  and  $Cs_1C_{60}$  spectra to the calculated density of states<sup>21</sup> for  $Rb_1C_{60}$  (bottom of Fig. 8) shows poor agreement with calculations that predict a total LUMO bandwidth (occupied and unoccupied) of  $\sim 0.6$  eV and an occupied portion of  $\sim 0.15$  eV. The discrepancy can be understood in terms of a transfer of

spectral weight away from  $E_F$  into the incoherent part of the spectral feature, as for  $A_3C_{60}$ . However, the  $A_1C_{60}$  phases exhibit emission consistent with a more standard Mott-Hubbard interpretation than for  $A_3C_{60}$ , suggesting more pronounced correlation effects. Within the framework of Mott-Hubbard theory, the energy necessary to remove an electron from one  $C_{60}$  molecule and place it on a neighboring molecule is the Hubbard  $U$ .  $U$  is estimated to be  $\sim 1.6$  eV for  $C_{60}$  (Refs. 29 and 30) and is approximately the same for  $A_6C_{60}$  (Ref. 30). When  $U$  is comparable to the width of the conduction band a pseudogap should open,<sup>26</sup> reducing the density of states at  $E_F$  and producing a broadened density of states below  $E_F$ , as observed for  $Rb_1C_{60}$  and  $Cs_1C_{60}$ .

The low carrier density of the  $Rb_1C_{60}$  and  $Cs_1C_{60}$  phases produces resistivities above the classic Mott limit for metals and measurements of the temperature coefficient of resistivity indicate nonmetallic character for  $x$  near 1.<sup>13</sup> From Fig. 8, however, there is emission at  $E_F$ , and such emission would normally suggest metallic character. This apparent paradox can be resolved by considering Anderson localization of the electronic states

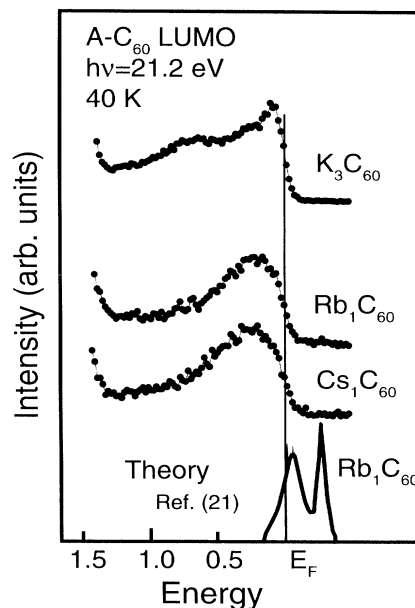


FIG. 8. LUMO emission from films of  $K_{2.2}C_{60}$ ,  $Rb_{0.7}C_{60}$ , and  $Cs_{0.8}C_{60}$  that are representative of the phases indicated. Each curve is normalized to its maximum intensity to emphasize line-shape changes. The  $A_1C_{60}$  phases show nearly Gaussian features  $\sim 0.5$  eV wide centered 0.25 eV below  $E_F$  with emission extending to  $E_F$ . In contrast, LDA calculations (Ref. 21) predict an occupied portion of the LUMO-derived band that is only  $\sim 0.15$  eV wide for  $Rb_1C_{60}$ . We attribute the difference to electron correlation effects that split the LUMO band and produce a dip at  $E_F$ . Comparison to transport results indicate that the electrons at  $E_F$  are localized, probably by merohedral disorder in the fullerene lattice. The LUMO emission for the K fullerides is characteristic of the  $A_3C_{60}$  phase with features 0.3 and 0.7 eV below  $E_F$  for  $0.1 \leq x \leq 2.2$  that fall outside the realm of LDA predictions.

surrounding  $E_F$ . Localization of what would ordinarily be the transport states is a result of disorder in the crystal lattice that interrupts the periodicity necessary for extended states. In the  $A_1C_{60}$  phases there are two possible sources of disorder, merohedral and ion position. Even when the  $C_{60}$  molecules are locked in position they are randomly distributed between two orientations (merohedral disorder). In addition, there may be vacancies in the octahedral sites that would contribute disorder, but little is known about the detailed filling for  $0 \leq x \leq 1$ . These interruptions in periodicity tend to localize electronic states near band edges, creating a mobility gap.<sup>26</sup> For increased electron densities (as in the  $A_3C_{60}$  phases), the Fermi level moves toward the middle of the LUMO-derived bands where there are delocalized states and metallic transport properties are obtained.

#### H. Occupation of LUMO+1 levels in $A-C_{60}$ systems

Figure 9 summarizes photoemission spectra for Na- $C_{60}$  systems prepared under different conditions. The top spectrum represents a  $Na_6C_{60}$  film produced by saturating a 200-Å fullerene film with Na vapor in ultrahigh vacuum. This spectrum demonstrates complete occupation of the LUMO levels and the preceding sections have shown equivalent spectra for the other saturated  $A_6C_{60}$  phases. Attempts to increase the stoichiometry by vacu-

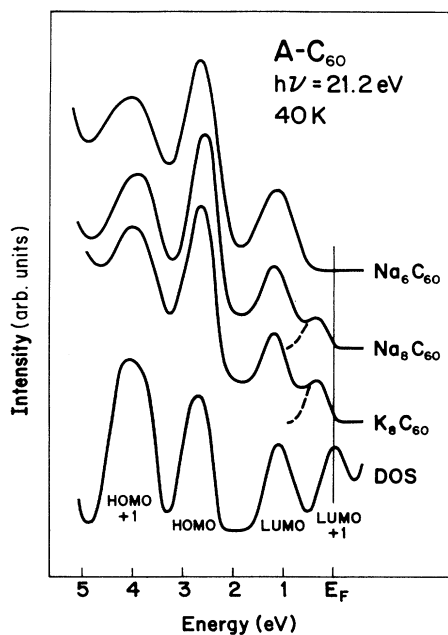


FIG. 9. Photoemission spectra for  $C_{60}$  molecules deposited on alkali-metal multilayers (center two curves) showing occupation of the fullerene LUMO+1 levels. Analysis of the emission intensity indicates the transfer of eight electrons per  $C_{60}$ . The abundance of alkali atoms and lack of steric hindrances to alkali-fullerene bonding suggest that this is an upper limit for charge transfer,  $C_{60}^{8-}$ . The top spectrum shows that LUMO is completely filled for a  $C_{60}$  film saturated with Na by vapor exposure and there is no LUMO+1 emission.

um vapor deposition for any alkali metal have failed. Yildirim *et al.*<sup>28</sup> recently achieved a higher doping level for Na- $C_{60}$  by growth in a closed thermodynamic system. They identified a  $Na_xC_{60}$  phase with a stoichiometry of  $x \sim 10$ , and suggested that this “superfulleride” might be superconducting as a result of partial occupation of the LUMO+1 band.

To create a condition where LUMO+1 occupation could be achieved and the coordination of  $C_{60}$  with alkali-metal atoms could be maximized, we condensed less than one monolayer of  $C_{60}$  onto alkali-metal films that were formed and held at 40 K. This low-temperature condensation process minimizes the tendency of the fullerenes to form an ordered array that would, in turn, introduce steric hindrance to alkali coordination. The middle photoemission spectrum of Fig. 9 shows that this process does indeed yield substantially higher electron charging of the fullerenes relative to the vapor exposed sample. Based on the emission intensity of the LUMO+1 states, we conclude that each fullerene has accepted eight electrons. The LUMO+1 feature appears symmetric, centered 0.8 eV above the LUMO and 0.4 eV below  $E_F$ . It is interesting to note that these superfulleride spectra contain sharp features even though deposition at 40 K must produce substantial disorder in the as-grown alkali-metal film and the fullerides themselves probably appear as  $C_{60}^{8-}$  states with a decoration of alkali-metal ions around them. This again implies that the  $C_{60}$  molecular states dictate the spectral signatures and the alkali act as charge donors, at least until  $x$  exceeds 8. The ease with which the fully coordinated  $C_{60}^{8-}$  structure forms demonstrates that the energetics of alkali-fullerene bonding favor a charge state greater than 6-. The inability to produce them in crystalline solids must be related to off-setting energies associated with lattice dilation. Only for Na is the octahedral hole sufficiently large to accommodate more than one ion.

The spectroscopic results show no increase in LUMO+1 occupation between Na and the more electropositive K and Rb atoms, as can be seen by comparing the middle two curves of Fig. 9. Thus, the heat of formation of the  $A_9C_{60}$  species is positive with respect to an  $A_8C_{60}$  species on an alkali-metal surface. The implication for  $Na_{10}C_{60}$  is that the atoms in the octahedral site are not all fully ionized but form hybrid states derived from Na and  $C_{60}$ . There must then be valence charge in the octahedral site and its character must be important in determining the physical properties of the  $Na_{10}C_{60}$  solid. We note that there is some analog in the superconducting  $Ca_5C_{60}$  structure where the LUMO+1 band is clearly hybridized with Ca  $s$  states.<sup>31</sup>

Finally, the photoemission spectra for  $Na_8C_{60}$  and  $K_8C_{60}$ , Fig. 9, show nearly zero emission at  $E_F$ , despite the fact that the molecular LUMO+1 level is sixfold degenerate and density-of-states calculations<sup>22</sup> (DOS, Fig. 9) would suggest a partially filled band for an  $A_8C_{60}$  crystal. The small emission at  $E_F$  can be attributed to the alkali-metal substrates. The low intensity is consistent with a much smaller photoemission cross section for the Na 3s and K 4s levels relative to the C  $2\pi$ -derived LUMO+1

level. The splitting of LUMO+1 may be a result of the highly asymmetric crystal field at the C<sub>60</sub>/alkali-metal interface.

#### IV. CONCLUSIONS

In this paper we have demonstrated that correlation plays an important role in the electronic properties of all alkali-metal fulleride phases. The A<sub>1</sub>C<sub>60</sub> phases formed for Rb and Cs are seen to be nonmetallic as a result of Andersen localization and exhibit LUMO emission broadened by correlation effects. Spectroscopic evidence indicates that the A<sub>4</sub>C<sub>60</sub> phases are Mott insulators and ordered A<sub>3</sub>C<sub>60</sub> films have metallic character. Highly ordered, well-annealed A<sub>3</sub>C<sub>60</sub> films show a LUMO-derived emission feature that has an apparent bandwidth ~4 times larger than predicted by band-structure calculations. The width of the LUMO-derived feature is a result

of electron-electron interaction since *U* and *W* are comparable and there is a feature ~0.7 eV below *E<sub>F</sub>* that is not represented in LDA calculations. Nonequilibrium growth is evident in all the fulleride systems. Temperature-dependent LEED studies show that the molecules on the C<sub>60</sub>(111) surface undergo a phase transition from simple cubic at low temperature to fcc at 230±20 K. Partial occupation of the (LUMO+1)-derived bands was achieved by depositing C<sub>60</sub> molecules on alkali-metal films.

#### ACKNOWLEDGMENTS

This work was supported by the National Science Foundation and by the Office of Naval Research. Discussions with D. M. Poirier, Y. B. Zhao, and M. Knupfer are gratefully appreciated as are XPS and STM results shared by D. M. Poirier and Y. B. Zhao.

- <sup>1</sup>For excellent reviews, see the articles in *Acc. Chem. Res.* **25**, (1992), and the special issue of *J. Phys. Chem. Solids* **53**, (1992).
- <sup>2</sup>P. A. Heiney, J. E. Fischer, A. R. McGhie, W. J. Romanow, A. M. Denenstien, J. P. McCauley, Jr., A. B. Smith III, and D. E. Cox, *Phys. Rev. Lett.* **66**, 2911 (1991); W. I. F. David *et al.*, *Nature* **353**, 147 (1991); D. A. Neumann *et al.*, *Phys. Rev. Lett.* **67**, 3808 (1991).
- <sup>3</sup>P. W. Stephens, L. Mihaly, J. B. Wiley, S.-M. Huang, R. B. Kaner, F. Diederich, R. L. Whetten, and K. Holczer, *Phys. Rev. B* **45**, 543 (1992); O. Zhou, J. E. Fischer, N. Coustel, S. Kycia, Q. Zhu, A. R. McGhie, W. J. Romanow, J. P. McCauley, Jr., A. B. Smith III, and D. E. Cox, *Nature* **351**, 462 (1991); Q. Zhu, O. Zhou, N. Coustel, G. B. M. Vaughan, J. P. McCauley, Jr., W. J. Romanow, J. E. Fischer, and A. B. Smith III, *Science* **254**, 545 (1991).
- <sup>4</sup>D. M. Poirier and J. H. Weaver, *Phys. Rev. B* **47**, 10959 (1993).
- <sup>5</sup>Q. Zhu, O. Zhou, N. Bykovetz, J. E. Fischer, A. R. McGhie, W. J. Romanow, C. L. Lin, R. M. Strongin, M. A. Cichy, and A. B. Smith III, *Phys. Rev. B* **47**, 13 948 (1993).
- <sup>6</sup>R. M. Fleming *et al.*, *Nature* **352**, 701 (1991).
- <sup>7</sup>R. Tycko, G. Dabbagh, D. W. Murphy, Q. Zhu, and J. E. Fischer, *Phys. Rev. B* (to be published).
- <sup>8</sup>R. Tycko, G. Dabbagh, M. J. Rosseinsky, D. W. Murphy, R. M. Fleming, A. P. Ramirez, and J. C. Tully, *Science* **253**, 884 (1991); S. E. Barrett and R. Tycko, *Phys. Rev. Lett.* **69**, 3755 (1992).
- <sup>9</sup>P. J. Benning, F. Stepniak, D. M. Poirier, J. L. Martins, J. H. Weaver, L. P. F. Chibante, and R. E. Smalley, *Phys. Rev. B* **47**, 13 843 (1993).
- <sup>10</sup>P. J. Benning, J. L. Martins, J. H. Weaver, L. P. F. Chibante, and R. E. Smalley, *Science* **252**, 1417 (1991); G. K. Wertheim, J. E. Rowe, D. N. E. Buchanan, E. E. Chaban, A. F. Hebard, A. R. Kortan, A. V. Makhija, and R. C. Haddon, *ibid.* **252**, 1419 (1991); C. T. Chen *et al.*, *Nature* **352**, 603 (1991); M. Merkel, M. Knupfer, M. S. Golden, J. Fink, R. Seemann, and R. L. Johnson, *Phys. Rev. B* **47**, 11 470 (1993); T. Takahashi *et al.*, *Phys. Rev. Lett.* **68**, 1232 (1992); P. J. Benning, D. M. Poirier, T. R. Ohno, Y. Chen, F. Stepniak, G. H. Kroll, J. H. Weaver, J. Fure, and R. E. Smalley, *Phys. Rev. B* **45**, 6899 (1992).
- <sup>11</sup>C. Gu, F. Stepniak, D. M. Poirier, M. B. Jost, P. J. Benning, Y. Chen, T. R. Ohno, J. L. Martins, J. H. Weaver, J. Fure, and R. E. Smalley, *Phys. Rev. B* **45**, 6348 (1992). Reevaluation of the Na-C<sub>60</sub> results suggests that the early measurements were adversely affected by oxygen contamination.
- <sup>12</sup>R. C. Haddon *et al.*, *Nature* **350**, 320 (1991); A. F. Hebard *et al.*, *ibid.* **350**, 600 (1991); M. J. Rosseinsky *et al.*, *Phys. Rev. Lett.* **66**, 2830 (1991); X.-D. Xiang, J. G. Hou, G. Briceño, W. A. Vareka, R. Mostovoy, A. Zettl, V. H. Crespi, and M. L. Cohen, *Science* **256**, 1190 (1992); T. T. M. Palstra, R. C. Haddon, A. F. Hebard, and J. Zaanen, *Phys. Rev. Lett.* **68**, 1054 (1992); H. Ogata *et al.*, *Jpn. J. Appl. Phys.* **31**, L166 (1992).
- <sup>13</sup>F. Stepniak, P. J. Benning, D. M. Poirier, and J. H. Weaver, *Phys. Rev. B* **48**, 1899 (1993).
- <sup>14</sup>J. H. Weaver, P. J. Benning, F. Stepniak, and D. M. Poirier, *J. Phys. Chem. Solids* **53**, 1707 (1992).
- <sup>15</sup>Y. Z. Li, J. C. Patrin, M. Chander, J. H. Weaver, L. P. F. Chibante, and R. E. Smalley, *Phys. Rev. B* **46**, 12 914 (1992).
- <sup>16</sup>Y. Zhao, D. M. Poirier, and J. H. Weaver, *J. Phys. Chem. Solids* (to be published); J. H. Weaver and D. M. Poirier, in *Fullerene Fundamentals*, edited by H. Ehrenreich and F. Spaepen, *Solid State Physics Vol. 48* (Academic, New York, in press), Chap. 1.
- <sup>17</sup>*Low Energy Electron Diffraction; The Theory and Its Application to the Determination of Surface Structure*, edited by J. B. Pendry (Academic, New York, 1974).
- <sup>18</sup>M. J. Rosseinsky, D. W. Murphy, R. M. Fleming, R. Tycko, A. P. Ramirez, T. Siegrist, G. Dabbagh, and S. E. Barrett, *Nature* **356**, 416 (1992).
- <sup>19</sup>*The Plastically Crystalline State; Orientationally-Disordered Crystals*, edited by J. N. Sherwood (Wiley, New York, 1979).
- <sup>20</sup>It is not possible to produce a film with a nominal stoichiometry near *x*=4 with negligible emission at *E<sub>F</sub>* without forming an insulating A<sub>4</sub>C<sub>60</sub> phase. If the spectra for *x* near 4 were obtained from a sample of mixed A<sub>3</sub>C<sub>60</sub> and A<sub>6</sub>C<sub>60</sub> phases, then ~67% of the sample would be A<sub>3</sub>C<sub>60</sub> and sizable emission would be present at *E<sub>F</sub>*.
- <sup>21</sup>S. Satpathy, V. P. Antropov, O. K. Andersen, O. Jepsen, O. Gunnarsson, and A. I. Liechtenstein, *Phys. Rev. B* **46**, 1773 (1992).
- <sup>22</sup>M.-Z. Huang, Y. N. Xu, and W. Y. Ching, *J. Chem. Phys.* **96**, 1648 (1992); J. L. Martins and N. Troullier, *Phys. Rev. B* **46**,

- 1766 (1992).
- <sup>23</sup>D. L. Lichtenberger *et al.*, in *Clusters and Cluster-Assembled Interfaces*, edited by R. S. Averback, J. Bernholc, and D. L. Nelson, MRS Symposia Proceedings No. 206 (Materials Research Society, Pittsburgh, 1991), p. 673.
- <sup>24</sup>A. Fujimori, I. Hase, H. Namatame, Y. Fujishima, Y. Tokura, H. Eisaki, S. Uchida, K. Takegahara, and F. M. F. de Groot, *Phys. Rev. Lett.* **69**, 1796 (1992).
- <sup>25</sup>A. Khurana, *Phys. Rev. B* **40**, 4316 (1989).
- <sup>26</sup>N. F. Mott, *Metal-Insulator Transitions*, 2nd ed. (Taylor & Francis, New York, 1990).
- <sup>27</sup>M. Knupfer, M. Merkel, M. S. Golden, J. Fink, O. Gunnarsson, and V. P. Antropov, *Phys. Rev. B* **47**, 13 944 (1993).
- <sup>28</sup>T. Yildirim, O. Zhou, J. E. Fischer, N. Bykovetz, R. A. Strongin, M. A. Cichy, A. B. Smith III, C. L. Lin, and R. Jelinek, *Nature* **360**, 568 (1992).
- <sup>29</sup>J. H. Weaver, *J. Phys. Chem. Solids* **53**, 1433 (1992).
- <sup>30</sup>R. W. Lof, M. A. van Veenendala, B. Koopmans, H. T. Jonkman, and G. A. Sawatzky, *Phys. Rev. Lett.* **68**, 3924 (1992).
- <sup>31</sup>Y. Chen, D. M. Poirier, M. B. Jost, C. Gu, T. R. Ohno, J. L. Martins, J. H. Weaver, L. P. F. Chibante, and R. E. Smalley, *Phys. Rev. B* **46**, 7961 (1992).

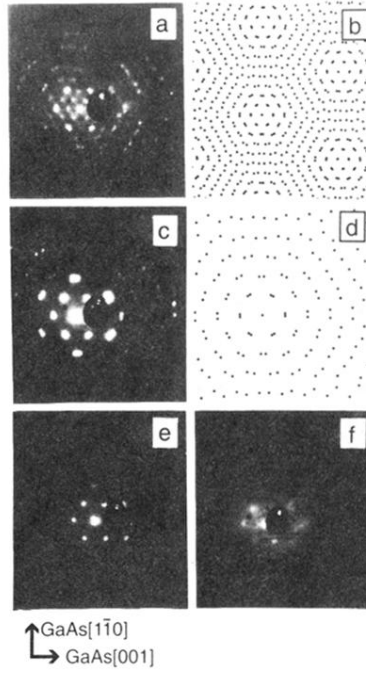


FIG. 1. LEED results at 40 K from a highly ordered K- $C_{60}$  film grown on GaAs(110) (electron energy 60 eV, film thickness 200 Å). (a) The hexagonal LEED pattern of  $K_{0.1}C_{60}$  is indicative of the simple-cubic lattice of  $C_{60}$  at 40 K. A moiré pattern is produced for growth on step-free surfaces because domains of  $C_{60}(111)$  can optimize substrate registry with  $[1\bar{1}0]$  oriented at  $\pm 3.5^\circ$  relative to GaAs $[1\bar{1}1]$ . This moiré pattern produces the dim and bright areas in (a) and the effect is modeled schematically in (b) where two simple-cubic arrays are rotated  $7^\circ$  relative to one another. (c) The LEED pattern for  $x = 2.2$  shows that the simple-cubic pattern is lost as the fcc  $K_3C_{60}$  pattern, characterized by the larger hexagons, increases. Again, the patterns from domains rotated  $\pm 3.5^\circ$  are clearly evident in (c). They are represented schematically in (d) where there are two spots for each hexagonal net position. The LEED pattern deteriorates as K concentration is increased to 2.8 and 3.7 and the  $K_3C_{60}$  grains are converted to body-centered  $K_4C_{60}$  grains.

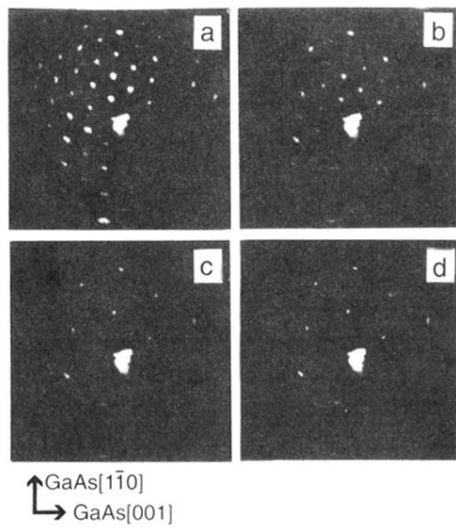


FIG. 2. (a)–(d) LEED results for undoped  $C_{60}$  at 40, 110, 200, and 230 K showing the washing out of the half-order spots with increasing temperature (electron energy 25 eV, film thickness 100 Å). The reduction is a consequence of increased librational motion above  $\sim 90$  K and the reduction in the simple-cubic order parameter.